ACS OMEGA

http://pubs.acs.org/journal/acsodf

Article

Essential Oils Extracted from *Boswellia sacra* Oleo Gum Resin Loaded into PLGA–PCL Nanoparticles: Enhanced Cytotoxic and Apoptotic Effects against Breast Cancer Cells

Hassan Mohamed El-Said Azzazy,* Anwar Abdelnaser, Hadeer Al Mulla, Amany M. Sawy, Samir N. Shamma, Mahmoud Elhusseiny, Salim Alwahibi, Noha Khalil Mahdy, and Sherif Ashraf Fahmy*

Cite This: *ACS Omega* 2023, 8, 1017–1025

Read Online

ACCESS | Metrics & More | Article Recommendations | Supporting Information

ABSTRACT: This work aims to develop and optimize blended polylactide-*co*-glycolide (PLGA) and poly(ε-caprolactone, PCL) loaded with *Boswellia sacra* oil (BO) to improve BO's physicochemical properties and anti-breast cancer effects *via* enhancing apoptosis. In this context, BO was extracted from *B. sacra* oleo gum resins (BO) *via* hydrodistillation and chemically characterized by evaluating its essential oil's composition using gas chromatography–mass spectrometry. Then, BO/PLGA–PCL NPs were formulated using the emulsion (O/W) solvent evaporation technique using a PLGA–PCL mixture at five different ratios (1:1, 2:1, 3:1, 1:2, and 1:3, respectively). The optimized NPs had a spherical morphology with no agglomerations and the lowest hydrodynamic size (230.3 ± 3.7 nm) and polydispersity index (0.13 ± 0.03) and the highest ζ potential (−20.36 ± 4.89 mV), as compared to the rest of the formulas. PLGA–PCL NPs could entrap 80.59 ± 3.37% of the BO and exhibited a controlled, sustained release of BO (83.74 ± 3.34%) over 72 h. Encapsulating BO in the form of BO/PLGA–PCL NPs resulted in a lower IC_{50} value as assessed by the MTT assay. Furthermore and upon assessing the apoptotic effect of both BO and BO/PLGA–PCL NPs, there was an increase in the percentage of apoptotic and necrotic cell percentages compared to the control and free BO. Encapsulation of BO in PLGA–PCL NPs doubled the percentage of apoptotic and necrotic cells exerted by free BO. These findings support the potential use of BO/PLGA–PCL NPs in treating breast cancer.

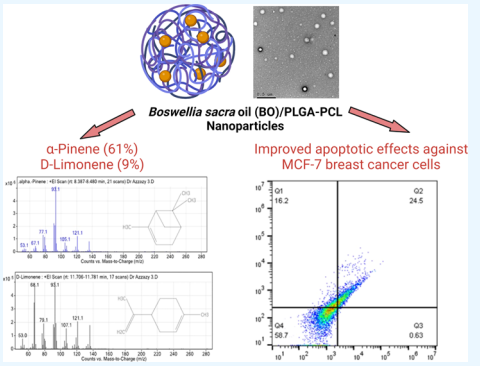

1. INTRODUCTION

Frankincense is an aromatic oleo gum resin generated by incising the tree trunks of the genus *Boswellia sacra* (family Burseraceae) grown perennially in Somalia, Oman, and Yemen.[1] Frankincense has been widely used in folk medicine in treating rheumatoid arthritis, urinary tract infections, bronchial asthma, pain, viral infections, and cancers.[1,2] Besides, the extracted oleo gum resin has been used in several industries, including perfume, food, beverage, cosmetics, and pharmaceuticals.[2] The broad biomedical applications of the gum resin frankincense are attributed to its high composition of hydrophobic mixtures of non-volatile and volatile constituents, including essential oils and boswellic acid monoterpenes.[3] Frankincense essential oils produced from *B. sacra* gum resins (BO) *via* hydrodistillation are reported to possess significant antiproliferative and anti-invasive activities against breast cancer and reduce neoplasm hostility in chemotherapy-resistant and metastatic breast cancer.[2] Another study reported the anticancer activity of frankincense oils against human pancreatic cancer *via* augmenting the caspase-dependent apoptotic pathway.[4] Moreover, frankincense oils were reported to have cytotoxic effects against colon cancer cells by suppressing cancer cell proliferation by decreasing β-catenin signaling molecules.[5] In addition, a case study reported the effectiveness of *B. sacra* resin against urothelial cancer when administrated *via* the oral route.[6] The anticancer activity of BO is attributed to its high content of volatile monoterpenes such as α-pinene, limonene, myrcene, α-thujene, *p*-cymene, and boswellic acid.[2] Despite their promising activities against various cancer cells, the clinical use of essential oils extracted from *B. sacra* is hindered by their hydrophobicity, poor bioavailability, and non-selective delivery to the tumor cells.[7] Several carrier systems were studied to accommodate numerous synthetic and natural compounds to increase their hydrophilicity and biological activities, including macromolecules,[8−10] chitosan nanoparticles,[11,12] nanovesicles (lipo-

Received: October 3, 2022
Accepted: December 8, 2022
Published: December 19, 2022

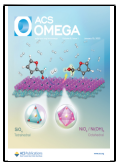

https://doi.org/10.1021/acsomega.2c06390
ACS Omega 2023, 8, 1017–1025

somes),[13] and biodegradable synthetic polymeric nanoparticles.[14]

Poly(ε-caprolactone) (PCL) is one of the most frequently used synthetic polymers in drug delivery because of its many advantages compared to other polymeric systems.[15] PCL is biodegradable and biocompatible and has a semicrystalline structure (resulting from its low glass transition temperature and high melting point), which increases its half-life in the systemic circulation. PCL also undergoes moderate degradation, leading to slow drug release. Additionally, PCL is relatively safe because its degradation does not generate acidic byproducts, unlike other polymers.[15,16] On the other hand, when used solely for drug delivery, PCL suffers a number of drawbacks, such as high hydrophobicity, poor stability in an aqueous solution, and rapid clearance by the reticuloendothelial system.[15,16] Thus, to overcome these drawbacks, PCL is usually modified with other hydrophilic polymers such as polylactide-*co*-glycolide (PLGA).[15] PLGA is another biocompatible and biodegradable synthetic polymer used to deliver various natural and synthetic drugs.[14,17] The use of PLGA as a carrier for biologically active drugs has several advantages, such as safety, complete and rapid drug release *via* the hydrolysis of its ester linkage, and improved bioavailability. In this context, PLGA and PCL were used to design nanocarriers that combine the advantages of both polymers to achieve the controlled release of loaded drugs.[18,19]

In this study, we formulated BO-loaded PLGA−PCL NPs (BO/PLGA−PCL NPs) and evaluated their potential effect on the breast cancer cell line MCF-7 cells. The essential oils were extracted from *B. sacra* oleo gum resins (BO) and chemically characterized by estimating the volatile oil content utilizing gas chromatography−mass spectrometry (GC−MS). BO/PLGA−PCL NPs were then designed using the emulsion (O/W) solvent evaporation technique employing PLGA−PCL mixtures at five different ratios (1:1, 2:1, 3:1, 1:2, and 1:3). The optimal formula, which exhibited the best hydrodynamic size, polydispersity index (PDI), ζ potential, and entrapment efficiency (EE %), was further characterized in terms of morphology, chemical composition, and release %. Furthermore, the effects of BO and BO/PLGA−PCL NPs on MCF-7 viability were compared. Additionally, the apoptotic effect of BO/PLGA−PCL NPs on MCF-7 cells was also investigated, in addition to their effect on cell cycle phases for possible use as an anticancer treatment.

2. MATERIALS AND METHODS

2.1. Materials. Poly(D,L-lactide-*co*-glycolide) (PLGA; 50:50) and PCL (molecular weight 40,000) were purchased from Sigma-Aldrich (St. Louis, MO). Polyvinyl alcohol (PVA; 98% hydrolyzed, MW ∼ 13,000) was purchased from Acros Organics (Geel, Belgium). Dimethylformamide and dichloromethane (DCM) were purchased from Fisher Chemicals (Fair Lawn, NJ). Dulbecco's modified Eagle's medium (DMEM) with 4.5 g/L glucose, 0.05% trypsin, and phosphate-buffered saline (PBS, pH 7.4) and DMEM without L-glutamine or phenol red and Trypan blue with 0.85% NaCl were purchased from Lonza Bioscience (Walkersville, MD). Dimethyl sulfoxide was obtained from Serva (Heidelberg, Germany). Annexin V-fluorescein isothiocyanate (FITC)/propidium iodide (PI) apoptosis detection kit was purchased from Elabscience (Wuhan, China). Ethanol and 3-(4,5-dimethylthiazol-2-yl)-2,5-diphenyltetrazolium bromide (MTT) were obtained from Thermo Fisher Scientific (Waltham, MA). Fetal bovine serum (FBS) was obtained from Gibco (Waltham, MA). MCF-7 cell lines (cat no. HTB-22) were purchased from ATCC (Manassas, VA). Other chemicals were obtained from Sigma-Aldrich (St. Louis, MO).

2.2. Extraction of Essential Oils from *B. sacra* Oleo Gum Resin (BO). Oleo gum resins were obtained from *B. sacra* plants grown in Oman and assembled in one lot. Briefly, hydrodistillation was carried out in a Milestone ETHOS X oven (Milestone, Italy) equipped with two 950 W magnetrons and an infrared temperature sensor. *B. sacra* resins were placed in distilled water at 100 °C in a ratio of 1:5 (w/v) and blended with an electromechanical agitator. The cooling system used was the Smart H150-2100 chiller (LabTech, MA), where the temperature and pressure of cooling water were set to 8 °C and 2.3 bar, respectively. The condenser was connected to the chiller, ensuring that the cooling water was at a constant temperature of 8 °C, and the extraction cycle was set to 45 min. The extracted liquid was collected in a 1 L bottle, and the volumes were recorded in a log for every cycle.

2.3. Analysis of the Chemical Composition of BO Utilizing GC−MS. GC−MS analysis was performed using Agilent Technologies gas chromatography (7890B) and a mass spectrometer detector (5977B). The GC was equipped with Agilent 19091S-433 UI and HP-5MS UI column (30 m × 0.25 mm internal diameter and 0.25 μm film thickness). Analyses were carried out using helium as the carrier gas at a flow rate of 1.0 mL/min in a split ratio of 30:1, injection volume of 1 μL, and the following temperature program: 40 °C for 1 min; raising at 4 °C/min to 150 °C and holding for 6 min; raising at 4 °C/min to 210 °C and holding for 1 min. The injector and detector were maintained at 280 and 220 °C, respectively. Mass spectra were obtained by electron ionization at 70 eV, using a spectral range of m/z 50−450 and solvent delay of 6 min. The sample run time was 50.5 min. Different constituents were identified by comparing the spectrum fragmentation pattern with those stored in the Wiley and NIST Mass Spectral Data Library.

2.4. Preparation and Optimization of PLGA−PCL NPs Loaded with BO (BO/PLGA−PCL NPs). BO/PLGA−PCL NPs were formulated using the emulsion (O/W) solvent evaporation technique, as described elsewhere, with some modifications.[19] A total weight of 30 mg of PLGA and PCL was used in five different ratios (1:1, 1:2, 1:3, 2:1, and 3:1, respectively). Briefly, 6 mg BO, PLGA, and PCL (30 mg) were dissolved in 1.2 mL of DCM at room temperature. Then, the obtained organic phase was added dropwise to 20 mL of 1.5% aqueous solution of the PVA while homogenizing at 11,000 rpm for 8 min in an ice bath. The resulting O/W emulsion was stirred with a magnetic stirrer for 5 h at room temperature to allow solvent evaporation and particle hardening. Afterward, the nanoparticle colloid was lyophilized for 72 h using a freeze dryer (TOPTION TOPT-10C freeze dryer, Toption Group Co., Limited, Xi'an, China). The dried NPs extract was stored in a desiccator at room temperature for further experiments.

2.5. Characterization of BO/PLGA−PCL NPs. *2.5.1. Particle Size, PDI, and ζ Potential Measurements.* The average particle size and ζ potential of NPs were determined using dynamic light scattering and laser Doppler velocimetry by using Zetasizer Nano ZS (Malvern Instruments, Worcestershire, UK), respectively.[20] All measurements took place at 25 °C in triplicate, and the results are expressed as mean ± standard deviation.

2.5.2. Entrapment Efficiency (EE %) of the BO/PLGA−PCL NPs. The EE % of the loaded BO into the PLGA−PCL NPs was determined *via* the direct method as described elsewhere with

https://doi.org/10.1021/acsomega.2c06390
ACS Omega 2023, 8, 1017−1025

some modifications.[10] Briefly, BO/PLGA−PCL NPs were centrifuged at 15,000 rpm and 4 °C for 3 h (Hermle Z 326 K, Labortechnik GmbH, Wehingen, Germany). Then, the pellet (containing the NPs) was separated and completely dissolved in a 1:1 DCM/dimethylformamide (DMF) mixture by vigorous vortex stirring. The amount of loaded BO was quantified, in the obtained clear solution, utilizing a FLUOstar Omega microplate reader (BMG Labtech, Offenburg, Germany) by measuring absorbance at 265 nm. The calibration curve was constructed using different concentrations (between 0.1 and 1.9 μg/mL) of the BO prepared by serial dilution using the solvent mixture (1 DCM/1 DMF). The resulting correlation coefficient (R^2) of the calibration curve was 0.9976. The EE % was computed using eq 1.[10]

$$\text{EE \%} = \frac{\text{total amount of loaded BO}}{\text{initial amount of BO}} \times 100 \quad (1)$$

2.5.3. Characteristics of the BO/PLGA−PCL NPs. The morphological structures of the BO/PLGA−PCL NPs were studied employing transmission electron microscopy (TEM, JEOL-JEM 2100 electron microscope, Musashino, Akishima, Tokyo, Japan) operating at 160 kV. A histogram demonstrating the average particle size of BO/PLGA−PCL NPs was constructed utilizing the image processing program ImageJ (NIH, Bethesda, MD).

The FTIR spectra of BO, PLGA−PCL, and BO/PLGA−PCL NPs were recorded and evaluated using attenuated total reflection Fourier-transformed infrared spectroscopy (ATR-FTIR) using an FTIR Nicolet 380 spectrometer (Thermo Scientific, Waltham, MA), equipped with a ZnSe flat crystal.[21] The spectra were determined by recording 64 transmission scans in the range of 4000 and 650 cm^{-1} with a resolution of 4 cm^{-1}.

2.5.4. In Vitro Release Study of BO from BO/PLGA−PCL NPs. The *in vitro* release rate of BO from BO/PLGA−PCL NPs was evaluated utilizing the dialysis bag method. Briefly, a known amount of the NPs was inserted into a dialysis bag (cutoff molecular weight, 12−14 kD). The dialysis bag was placed in 25 mL of phosphate buffer saline (PBS, pH 7.4) supplemented with 1.5% Tween 80 and 0.5% FBS in a shaking incubator (Jeio Tech SI-300, Seoul, Korea), rotating at 300 rpm at 37 °C. At specific time intervals, a 1 mL aliquot of the sample was withdrawn and immediately replaced with an equivalent volume of warmed buffer solution. The amount of the released BO was quantified in the withdrawn sample using a FLUOstar Omega microplate reader at 265 nm. The release percentage (%) was calculated using eq 2.

$$\text{Release \%} = \frac{\text{amount of released BO}}{\text{initial amount of loaded BO}} \times 100 \quad (2)$$

2.5.5. Cell Viability Assay. 2.5.5.1. Cell Culture. Human breast adenocarcinoma (MCF-7) cells (HTB-22; ATCC, Manassas, VA) were maintained in DMEM supplemented with 5% penicillin−streptomycin and 10% FBS and incubated at 37 °C and 5% CO_2. Cells were stained with Trypan blue, and the viable cell count was determined using a hemocytometer. For the MTT assay, MCF-7 cells were seeded in 96-well plates at a seeding density of 1×10^4 cells/well.

2.5.5.2. MTT Assay. MCF-7 cells were cultured in DMEM supplemented with 10% FBS and 1% penicillin−streptomycin and maintained at 37 °C in a humidified atmosphere with 5% CO_2.

The viability of MCF-7 cells was assessed by using the MTT assay. The cells were seeded in 96-well plates at a density of 1×10^4 cells/well and incubated for 24 h at 37 °C under 5% CO_2. Then, cells were washed with PBS and co-incubated with BO or BO/PLGA−PCL NPs for 24 h at concentrations of 0.19, 0.39, 0.78, 1.56, 3.12, and 6.25 μg/mL. After that, 50 μL of MTT solution was added to each well and incubated for 4 h. Then, 150 μL of SDS solution was added and incubated further for 2 h. After the blue formazan crystals were dissolved, the absorbance of each well was measured at 570 nm using a microplate reader (Bio-Tek 800TS). Untreated cells were used as control.

2.5.6. Flow Cytometry and Cell Cycle Analysis. After the confluency of the MCF-7 cells reached 80%, cells were harvested and re-seeded in a 6-well plate. Once the confluency reached 60%, cells were treated for 24 h with IC_{50} concentrations of tested formulas, as indicated in Table 3. The plates were then washed 3 times with washing buffer, assessed for viability using Trypan blue exclusion dye, and finally stained with PI and Annexin V-PE according to the manufacturer's instructions and analyzed using a flow cytometer (Attune NxT, Thermo Fisher Scientific, Waltham, MA).

PI reading was deducted from FITC-negative and FITC-positive cells, to determine viable and early apoptotic cells sequentially. Cell cycle analysis was performed after staining cells with PI. The DNA content of cells was measured by flow cytometry and then processed by FlowJo software Version 10.6.2. A singlet gate was used to exclude doublets and aggregates that might have formed during the staining processes. The analysis for all flow cytometry data was performed using FlowJo software Version 10.6.2 (Treestar, OR).

2.5.7. Statistical Analysis. All experiments were conducted in triplicate, and the results are expressed as mean ± standard deviations. Statistical analysis was performed by GraphPad Prism software version 8.0 (GraphPad, San Diego, CA) using a one-way ANOVA test, considering the difference statistically significant when the *p*-value was <0.05.

3. RESULTS AND DISCUSSION

3.1. Analysis of the Chemical Composition of BO Utilizing GC−MS. The GC−MS chromatogram analysis of BO indicated the presence of 32 compounds (Figure 1). Comparing

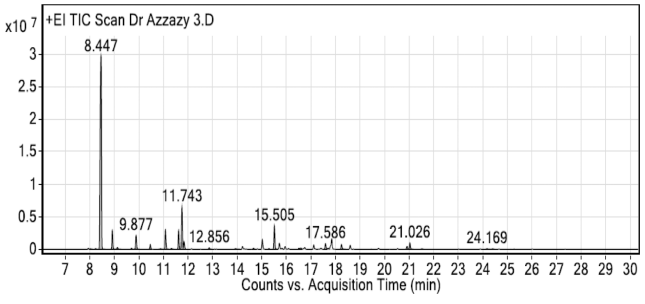

Figure 1. GC−MS chromatogram of BO extracted from *B. sacra* oleo gum resin.

the mass spectra of the constituents with the NIST library, essential oil compositions were identified, characterized, and then recognized, as presented in Table 1. The GC−MS analysis revealed that the most abundant compound in the BO is α-pinene (61.05%), while the second most abundant compound is D-limonene (9%). The chemical structures and mass spectra of

https://doi.org/10.1021/acsomega.2c06390
ACS Omega 2023, 8, 1017−1025

Table 1. Chemical Composition of Volatile Oil Extracted from BO

peak no.	RT	compound name	%
		Monoterpenes	
1	8.024	tricyclene	0.11
2	8.229	α-thujene	0.13
3	8.447	α-pinene	61.05
4	8.908	camphene	3.67
5	9.118	verbenene	0.43
6	9.69	p-cymene	0.25
7	9.798	sabinene	0.09
8	9.877	β-pinene	2.83
9	10.454	β-myrcene	0.94
10	10.873	α-phellandrene	0.16
11	11.073	δ-3-carene	4.22
12	11.189	p-cymenene	0.06
13	11.32	α-terpinene	0.19
14	11.608	o-cymene	3.57
15	11.743	D-limonene	9
17	12.856	γ-terpinene	0.35
24	17.586	alloocimene	1.35
29	21.52	R(+)-limonen	0.11
		total	**88.51**
		Oxygenated Monoterpenes	
16	11.827	eucalyptol	1.7
18	13.922	*trans*-D-dihydrocarveol	0.22
20	15.286	6-camphenol	0.19
21	15.505	2,3-epoxycarane, (*E*)-	4.86
22	16.506	verbenol	0.24
23	16.585	pinocarvone	0.33
25	18.238	verbenone	1.18
26	19.453	carvone	0.06
		total	**8.78**
		Esters	
27	20.905	bornyl acetate	0.66
28	21.026	bicyclo[2.2.1]heptane-3-methylene-2,2-dimethyl-5-ol acetate	1.44
		total	**2.1**
		Sesquiterpenes	
30	24.169	β-bourbonene	0.17
31	24.401	β-elemene	0.11
32	25.267	caryophyllene	0.07
		total	**0.35**
		Others	
19	14.658	6-isopropenyl-3-methoxymethoxy-3-methyl-cyclohexene	0.25

α-pinene and D-limonene are illustrated in Figure 2A,B, respectively.

Also, the GC−MS analysis of BO showed the presence of monoterpenes (88.51%), oxygenated monoterpenes (8.78%), esters (2.1%), and sesquiterpenes (0.35%), as presented in Figure 1 and Table 1.

3.2. Characterization of the BO/PLGA−PCL NPs.

3.2.1. Hydrodynamic Particle Size, PDI, ζ Potential, and Entrapment Efficiency (EE %). Different ratios of PLGA and PCL (1:1, 2:1, 3:1, 1:2, and 1:3) were assessed to design the BO/PLGA−PCL NPs. The best-optimized formulation with respect to hydrodynamic size, PDI, ζ potential, and EE % was selected for further experiments. The average hydrodynamic sizes, PDI, ζ potential, and EE % of the BO/PLGA−PCL NP formulations prepared using different PLGA−PCL ratios are presented in Table 2. The BO/PLGA−PCL NPs formulated using PLGA/PCL in a ratio of 1:1 (P1 formula) had the lowest hydrodynamic size (230.3 ± 3.7 nm) and PDI (0.13 ± 0.03) and the highest ζ potential (−20.36 ± 4.89 mV), as compared to the rest of the formulas (P2, P3, P4, and P5). The small size of P1 would facilitate the passive accumulation of NPs in tumor tissues with permeable vasculature and deprived lymphatic drainage.[11] Moreover, the small PDI value of the P1 formula indicates the unimodal and narrow particle size distribution where the NPs are homogeneously and uniformly distributed.[22] Additionally, the high negative surface charge of the P1 formula would prevent NP clumping and improve their stability for an extended period.[23]

Furthermore, the P1 formula exhibited a higher EE % (80.59 ± 3.37%) as compared to other formulas, which is possibly credited to its smaller particle size (230 ± 3.7 nm). The greater surface area-to-volume ratio of the P1 formula enabled higher entrapment of BO containing the two major monoterpenes (α-pinene and D-limonene), which have been reported to have strong anticancer activities.[23]

3.2.2. Morphological and Chemical Characteristics of BO/PLGA−PCL NPs. TEM was used to study the morphology and average size of the BO/PLGA−PCL NPs (prepared using a 1:1 ratio of PLGA−PCL). As demonstrated in Figure 3A, the NPs exhibited a spherical morphology with no observed agglomeration. The average size of the optimal BO/PLGA−PCL NP formula was computed using an image processing program (ImageJ, NIH, Bethesda, MD) and was found to be 88.67 ± 20.68 nm (Figure 3B).

The ATR-FTIR spectrum of BO (Figure 4A) demonstrated three distinctive peaks at 2919 cm^{-1} (C−H stretching), 1440 cm^{-1} (C−H bending), and 1361 cm^{-1} (C−O stretching).[24] On the other hand, the spectrum of the PLGA−PCL NP blank formula (Figure 4B) exhibited four peaks at 3305 cm^{-1} (OH stretching), 2931 cm^{-1} (C−H bending), 1727 cm^{-1} (C═O stretching), and 1094 cm^{-1} (C−O stretching).[25] The principal peaks of BO and blank PLGA−PCL NPs existed in the spectrum of BO/PLGA−PCL NPs (Figure 4C), with negligible apparent shifts, proposing the physical loading of BO within the polymeric matrix.[26]

3.2.3. In Vitro Release Study. Figure 5 demonstrates the release % of unloaded BO and BO from the BO/PLGA−PCL NPs into the PBS medium at 37 °C. BO exhibits almost complete diffusion (96.9 ± 1.90%) from the dialysis membrane within 6 h. On the other hand, BO showed a sustained release behavior over 72 h, where 40.86 ± 2.86 and 83.74 ± 3.34% were diffused from the dialysis bag after 6 and 72 h at pH 7.4, respectively. At the pH of the cancer cells' extracellular fluid (pH of 5.5), BO showed a rapid release behavior over 72 h, where 59.16 ± 2.35 and 92.49 ± 3.70% were diffused from the dialysis bag after 6 and 72 h, respectively. Blending PLGA with PCL has achieved a controlled, sustained manner where a balance between release rates occurs. Using PLGA leads to rapid diffusion of the loaded BO from the polymeric matrix *via* polymer swelling after exposure to the PBS, resulting in erosion of the polymeric matrix.[27] Additionally, the cleavage of the ester linkage in the PLGA leads to the rapid release of the BO.[27] On the other hand, using PCL results in slow diffusion rates out of the polymeric matrix due to its semicrystalline and hydrophobic nature, leading to the slow hydrolysis of the polymer and prolonged release of the loaded drug.[28] In this regard, designing polymeric NPs by blending PLGA−PCL polymers leads to moderate release rates of the loaded drug.

https://doi.org/10.1021/acsomega.2c06390
ACS Omega 2023, 8, 1017−1025

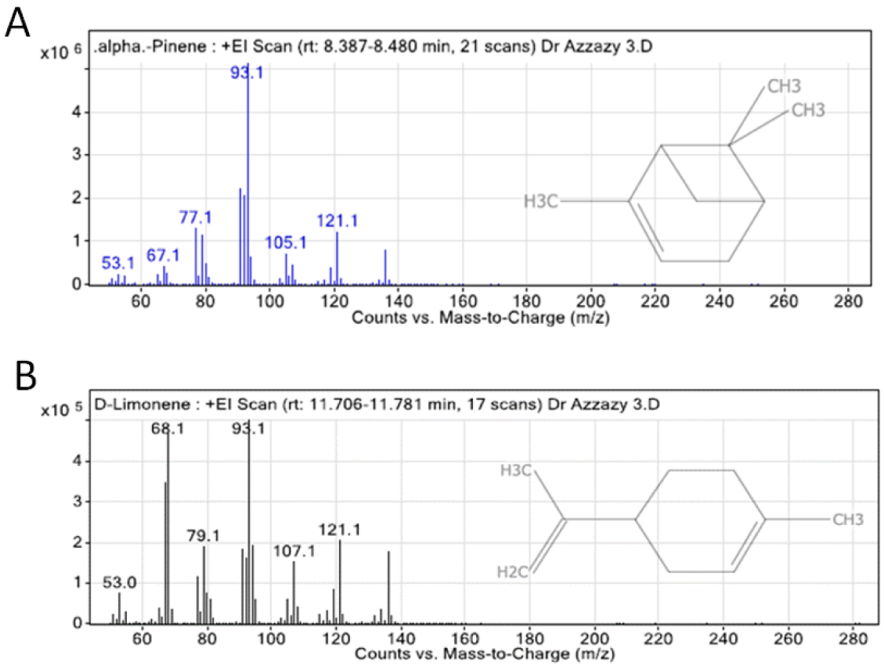

Figure 2. Chemical structure and mass spectrum of (A) α-pinene and (B) D-limonene.

Table 2. Average Particle Sizes, PDI, ζ Potential, and EE % of Different BO/PLGA−PCL NP Formulas

	ratio					
formula code	PLGA	PCL	hydrodynamic size (nm)	PDI	ζ potential (mV)	EE %
P1	1	1	230.3 ± 3.7	0.13 ± 0.03	−20.36 ± 4.89	80.59 ± 3.37
P2	2	1	567.5 ± 35.55	0.96 ± 0.08	−5.69 ± 2.79	73.17 ± 4.20
P3	3	1	1463.7 ± 159.6	0.56 ± 0.004	−5.66 ± 2.02	36.34 ± 4.21
P4	1	2	1174.0 ± 148.9	0.66 ± 0.3	−2.84 ± 1.11	27.04 ± 1.08
P5	1	3	1025.4 ± 120.4	0.76 ± 0.2	−1.89 ± 0.57	43.15 ± 3.90

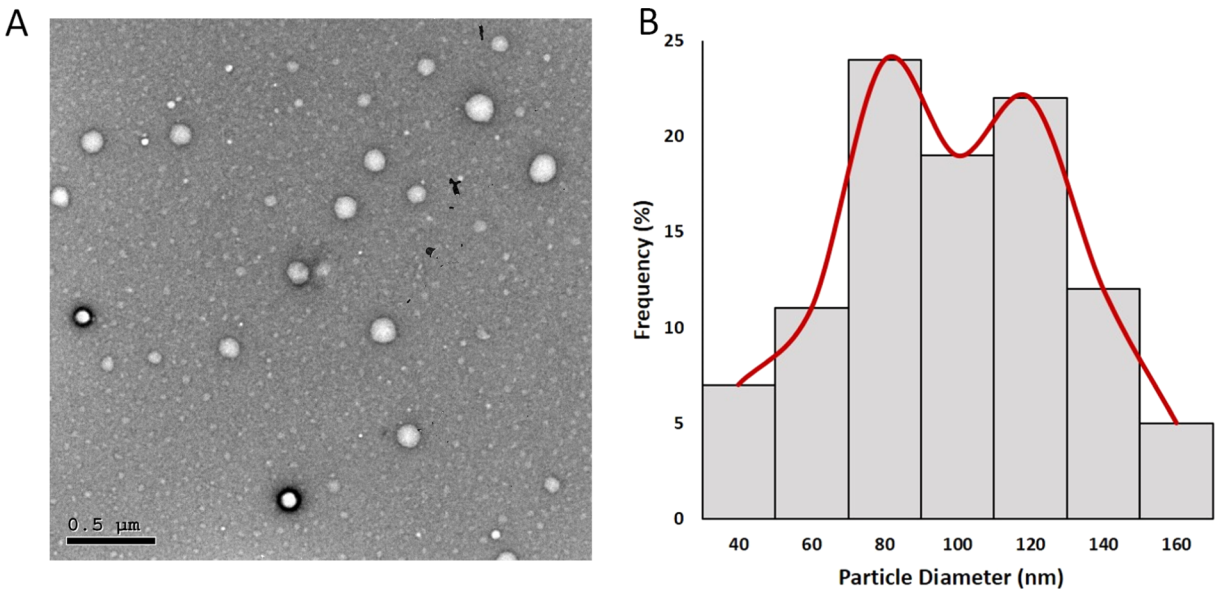

Figure 3. (A) TEM images of the optimal BO/PLGA−PCL NPs. (B) the particle size (nm) histogram of the optimal BO/PLGA−PCL NPs was generated employing the ImageJ program.

3.2.4. Cytotoxicity Assay. The cytotoxic effects of BO and BO/PLGA−PCL NPs were examined using MTT assay. PLGA−PCL NPs alone had no significant cytotoxicity on MCF-7 up to 200 μg/mL (Figure S1), eliminating the probability that the reduced cell survival in the BO/PLGA−PCL NP treatments is due to the void NPs. BO/PLGA−PCL NPs showed enhanced cytotoxicity against MCF-7 cells compared to the free BO (Figure 6 and Table 3). In particular,

https://doi.org/10.1021/acsomega.2c06390
ACS Omega 2023, 8, 1017−1025

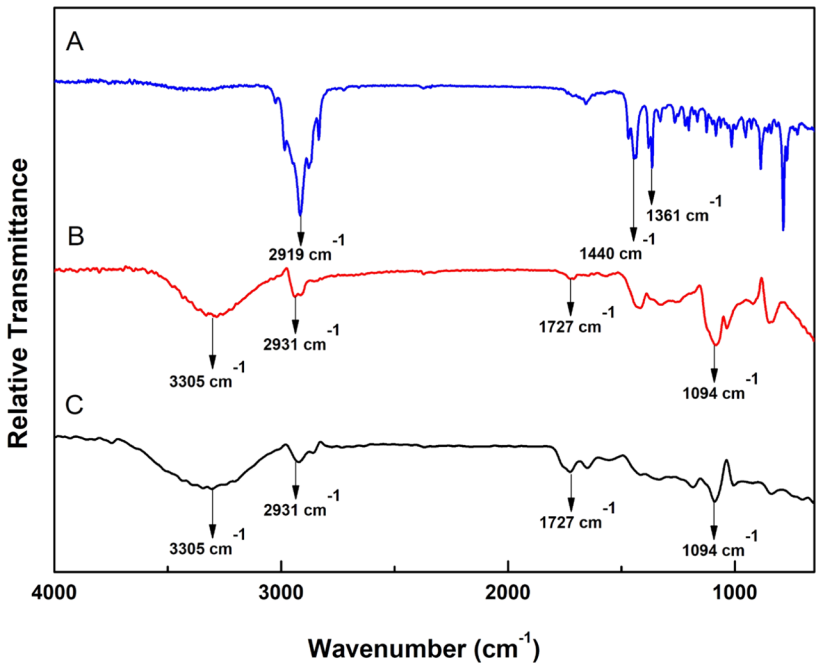

Figure 4. FTIR spectra of (A) *B. sacra* resin oil (BO), (B) blank PLGA−PCL NPs, and (C) BO/PLGA−PCL NPs.

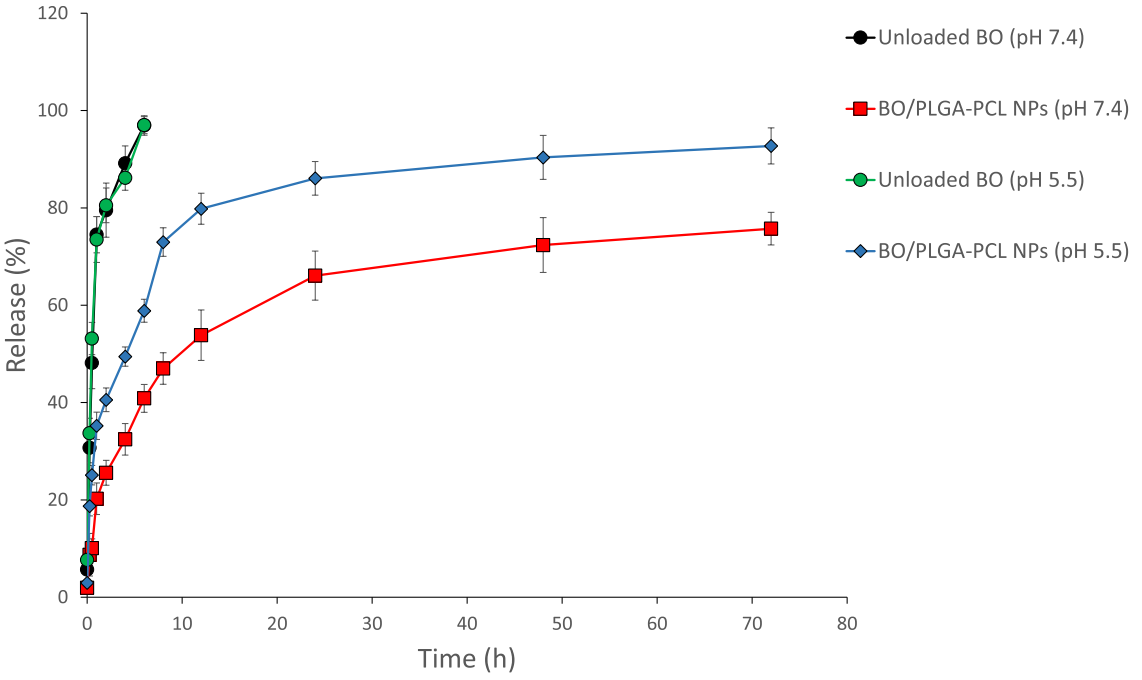

Figure 5. Time-dependent release % of unloaded BO and BO from BO/PLGA−PCL NPs at 37 °C, into phosphate buffer (pH 7.4 and 5.5).

BO showed increased cytotoxicity of 3.54 ± 1.4, 7.2 ± 0.06, 13.37 ± 4.1, 32.8 ± 2.4, 24.01 ± 2.7, 59.29 ± 5.1, and 36.48 ± 5.2%, at 0.19, 0.39, 0.78, 1.56, 3.12, and 6.25 μg/mL, respectively, compared to control (Figure 6). Interestingly, when cells were treated with BO/PLGA−PCL NPs at the same concentrations, the cytotoxicity increased to 33.59 ± 3.3, 35.4 ± 0.5, 44.81 ± 2.6, 54.40 ± 2.1, and 64.17 ± 0.2%, respectively, compared to control (Figure 6). It was evident that encapsulation of BO in PLGA−PCL NPs significantly increased cellular cytotoxicity when compared to the corresponding concentration of free BO. It was previously demonstrated that BO significantly reduced the cellular viability of MCF-7, MDA-MB-23, and T47D human breast cancer cell lines due to its high content of monoterpenes (such as α-pinene and D-limonene).[29] This effect was not limited to the breast cancer cells, as BO had a similar effect on reducing the cellular viability of other cancer cell lines, such as human bladder cancer J82 cells.[30] Interestingly, when these cytotoxic effects were tested on non-cancer cell lines such as the human embryonic kidney cells HEK-293, normal breast cells MCF10-2A, and normal bladder urothelial cells UROtsa, there was no significant effect on the cellular viability, suggesting that this effect is sustained only in the presence of cancer cells but not normal cells.[31] While on its own, it was evident that BO had a significant impact on the cellular viability

https://doi.org/10.1021/acsomega.2c06390
ACS Omega 2023, 8, 1017−1025

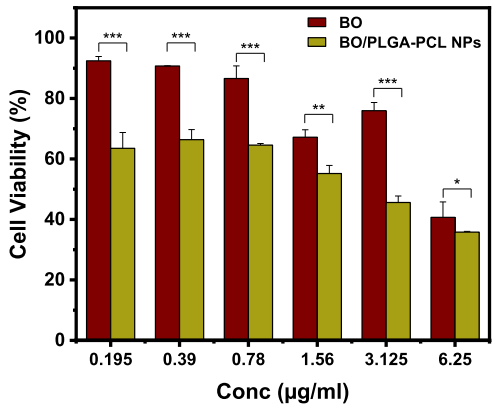

Figure 6. Cytotoxicity of BO and BO/PLGA−PCL NPs on MCF-7 cells treated with BO and BO/PLGA−PCL NPs at 24 h incubation time. Data are presented as mean ± SD from three independent experiments. *$P \leq 0.05$, **$P \leq 0.01$, ***$P \leq 0.001$. Blank PLGA−PCL NPs exhibited negligible cytotoxicity.

Table 3. IC_{50} Values for PLGA−PCL NPs, Free BO, and BO/PLGA−PCL NPs

formula	IC_{50} (μg/mL)
PLGA−PCL NPs	>200
BO	9.55 ± 0.7
BO/PLGA−PCL NPs	2.32 ± 0.49(**$P \leq 0.01$ as compared to the BO)

of MCF-7 cells, it was important to increase its potency by encapsulation in PLGA−PCL NPs. Our results are in agreement with previously published data that showed an increase in the potency of other treatments upon encapsulating them in PLGA−PCL NPs.[32] α-Pinene has been reported to activate natural killer lymphocytes which recognize and kill cancer cells *via* activation of apoptosis.[33] On the other hand, D-limonene has been shown to directly exert multiple pharmacological activities against cancer cells including reduction of growth and chemoresistance of cancer cells.[34]

3.2.5. Flow Cytometry. Based on our results of the MTT assay on MCF-7 and in order to dissect the mode of cell death in response to free BO and BO/PLGA−PCL NPs, MCF-7 cells were treated with the IC_{50} concentration of both BO and BO/PLGA−PCL NPs for 24 h. Thereafter, cells were stained with Annexin V and PI to assess the percentages of the apoptotic and necrotic cells. The analysis for all flow cytometry data was performed using FlowJo software Version 10.6.2 (Treestar, OR) and as described previously.[35] Our results indicate that BO alone was able to increase the percentage of apoptotic cells by 12.7% and the percentage of necrotic cells by 7.4% compared to the control (Figure 7). Importantly, when cells were treated with the IC_{50} concentration of BO/PLGA−PCL NPs, the percentage of apoptotic cells increased to 24.5% and the percentage of necrotic cells increased to 16.2% compared to the control (Figure 7). While our results are in agreement with previously published studies showing that BO induces apoptosis in different breast cancer cell lines such as T47D, MCF7, and MDA-MB-231, the previously published work assessed apoptosis using the DNA fragmentation technique rather than the currently employed flow cytometric method, which gives a better assessment of the phases of apoptosis in addition to necrosis.[29] Interestingly, and to the best of our knowledge, there have been no previous reports assessing the apoptotic effects of BO and comparing it to a nano-formulation in which BO was specifically encapsulated in PLGA−PCL NPs.

3.2.6. Cell Cycle Analysis. Although the apoptotic effects of BO and BO/PLGA−PCL NPs were assessed, it was still important to examine whether there has been any effect on cellular proliferation. It was previously shown that BO affects different cell cycle regulators. As can be seen from the cell cycle analysis (Table 4), it is evident that both BO and BO/PLGA−PCL NPs do exert a cell cycle arrest yet at a different stage, which indicates a differential cell cycle arrest mechanism between the two treatments. The BO/PLGA−PCL NPs arrested cells at the G0−G1 phase, as most of the cells accumulate at this stage

Table 4. Effects of BO and BO/PLGA−PCL NPs on MCF-7 Cell Cycle Arrest

	DNA phase		
sample	G0−G1	S	G2/M
control	50.5	14.4	35.1
BO	62.6	22.2	15.1
BO/PLGA−PCL NPs	84.6	8.2	7.2

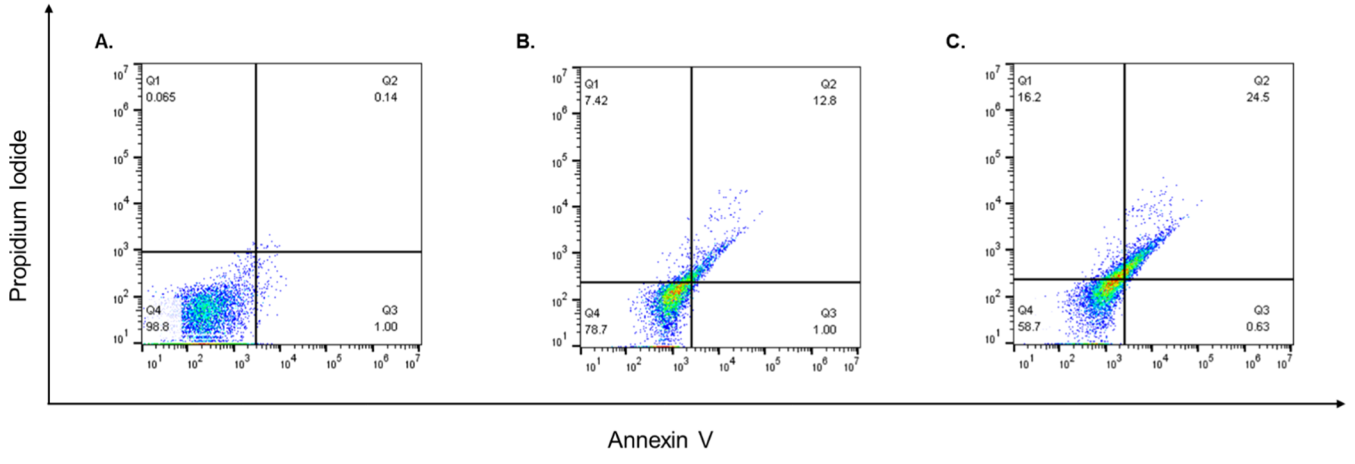

Figure 7. Apoptotic effects of BO and BO/PLGA−PCL NPs. MCF-7 cells were treated for 24 h with (A) vehicle (DMEM), or IC_{50} concentrations of (B) BO or (C) BO/PLGA−PCL NPs. Thereafter, the percentages of viable, early, and late apoptotic cells were detected *via* Annexin/PI staining that was measured using the flow cytometric analysis.

https://doi.org/10.1021/acsomega.2c06390
ACS Omega 2023, 8, 1017−1025

(84%). However, BO arrested the cells at the G0−G1 phase in addition to the S phase as both had higher percentages of cells compared to control cells. Similar to the previous findings, previous reports have shown that BO affects cell cycle regulators such as cdk4 and cyclin D1.[29] However, it was not demonstrated previously at which stage BO arrested the cells or what would be the effect of encapsulating BO in PLGA−PCL NPs.

4. CONCLUSIONS

In this study, the essential oils were extracted from *B. sacra* oleo gum resins (BO), chemically characterized by GC−MS analysis, and loaded into polymeric nanoparticles comprising a mixture of PLGA−PCL forming BO/PLGA−PCL NPs. Five different ratios of PLGA and PCL (1:1, 2:1, 3:1, 1:2, and 1:3, respectively) were evaluated in terms of hydrodynamic size, PDI, ζ potential, and EE % to select the best-optimized formula. The optimal BO/PLGA−PCL NPs (1:1) had the smallest size and PDI and the highest surface charge and EE %. Additionally, they exhibited a controlled release of encapsulated BO over a period of 72 h. With regard to their effect on MCF-7 cellular apoptosis and cell cycle arrest, it is plausible to conclude that although there is an increase in the apoptotic and necrotic cell populations upon the treatment of MCF-7 cells with BO/PLGA−PCL NPs in comparison to free BO, it is evident that this increase was not only quantitatively different but also qualitatively different as the effect on the cell cycle arrest was different between the two treatments.

■ ASSOCIATED CONTENT

Supporting Information

The Supporting Information is available free of charge at https://pubs.acs.org/doi/10.1021/acsomega.2c06390.

Cell viability of MCF-7 cells after treatment with PLGA−PCL NPs for 24 h (PDF)

■ AUTHOR INFORMATION

Corresponding Authors

Hassan Mohamed El-Said Azzazy − *Department of Chemistry, School of Sciences & Engineering, The American University in Cairo, New Cairo 11835, Egypt; Department of Nanobiophotonics, Leibniz Institute for Photonic Technology, Jena 07745, Germany;* orcid.org/0000-0003-2047-4222; Phone: +2 02 2615 2559; Email: hazzazy@aucegypt.edu

Sherif Ashraf Fahmy − *Department of Chemistry, School of Sciences & Engineering, The American University in Cairo, New Cairo 11835, Egypt; Chemistry Department, School of Life and Medical Sciences, University of Hertfordshire Hosted by Global Academic Foundation, Cairo 11835, Egypt;* orcid.org/0000-0003-3056-8281; Phone: +201222613344; Email: sheriffahmy@aucegypt.edu

Authors

Anwar Abdelnaser − *Institute of Global Health and Human Ecology, School of Sciences & Engineering, The American University in Cairo, New Cairo 11835, Egypt*

Hadeer Al Mulla − *Department of Chemistry, School of Sciences & Engineering, The American University in Cairo, New Cairo 11835, Egypt*

Amany M. Sawy − *Department of Chemistry, School of Sciences & Engineering, The American University in Cairo, New Cairo 11835, Egypt*

Samir N. Shamma − *Institute of Global Health and Human Ecology, School of Sciences & Engineering, The American University in Cairo, New Cairo 11835, Egypt*

Mahmoud Elhusseiny − *Institute of Global Health and Human Ecology, School of Sciences & Engineering, The American University in Cairo, New Cairo 11835, Egypt*

Salim Alwahibi − *Falha Medical Solutions, Muscat 113, Oman*

Noha Khalil Mahdy − *Department of Chemistry, School of Sciences & Engineering, The American University in Cairo, New Cairo 11835, Egypt*

Complete contact information is available at: https://pubs.acs.org/10.1021/acsomega.2c06390

Notes

The authors declare no competing financial interest.

■ ACKNOWLEDGMENTS

This work was funded by a grant from the American University to Prof. Hassan Azzazy.

■ REFERENCES

(1) Di Stefano, V.; Schillaci, D.; Cusimano, M. G.; Rishan, M.; Rashan, L. In Vitro Antimicrobial Activity of Frankincense Oils from *Boswellia sacra* Grown in Different Locations of the Dhofar Region (Oman). *Antibiotics* **2020**, *9*, 195.

(2) Khajehdehi, M.; Khalaj-Kondori, M.; Baradaran, B. Molecular evidences on anti-inflammatory, anticancer, and memory-boosting effects of frankincense. *Phytother. Res.* **2022**, *36*, 1194−1215.

(3) Miran, M.; Amirshahrokhi, K.; Ajanii, Y.; Zadali, R.; Rutter, M. W.; Enayati, A.; Movahedzadeh, F. Taxonomical Investigation, Chemical Composition, Traditional Use in Medicine, and Pharmacological Activities of Boswellia sacra Flueck. *Evidence-Based Complementary Altern. Med.* **2022**, *2022*, 8779676.

(4) Ni, X.; Suhail, M. M.; Yang, Q.; Cao, A.; Fung, K. M.; Postier, R. G.; Woolley, C.; Young, G.; Zhang, J.; Lin, H. K. Frankincense essential oil prepared from hydrodistillation of *Boswellia sacra* gum resins induces human pancreatic cancer cell death in cultures and in a xenograft murine model. *BMC Complementary Altern. Med.* **2012**, *12*, 253.

(5) Becer, E.; Kabadayı, H.; Başer, K. H. C.; Vatansever, H. S. Boswellia sacra essential oil manages colon cancer stem cells proliferation and apoptosis: a new perspective for cure. *J. Essent. Oil Res.* **2021**, *33*, 53−62.

(6) Xia, D.; Lou, W.; Fung, K. M.; Wolley, C. L.; Suhail, M. M.; Lin, H. K. Cancer chemopreventive effects of Boswellia sacra gum resin hydrodistillates on invasive urothelial cell carcinoma: report of a case. *Integr. Cancer Ther.* **2017**, *16*, 605−611.

(7) Johnson, S.; DeCarlo, A.; Satyal, P.; Dosoky, N. S.; Sorensen, A.; Setzer, W. N. The chemical composition of Boswellia occulta oleogum resin essential oils. *Nat. Prod. Commun.* **2019**, *14*, 1934578X1986630.

(8) Fahmy, S. A.; Ponte, F.; Fawzy, I. M.; Sicilia, E.; Bakowsky, U.; Azzazy, H. M. E.-S. Betaine host−guest complexation with a calixarene receptor: enhanced in vitro anticancer effect. *RSC Adv.* **2021**, *11*, 24673−24680.

(9) Fahmy, S. A.; Ponte, F.; Sicilia, E.; El-Said Azzazy, H. M. Experimental and Computational Investigations of Carboplatin Supramolecular Complexes. *ACS Omega* **2020**, *5*, 31456−31466.

(10) Fahmy, S. A.; Brüßler, J.; Ponte, F.; Abd El-Rahman, M. K.; Russo, N.; Sicilia, E.; Bakowsky, U.; Shoeib, T. A study on the physicochemical properties and cytotoxic activity of p-sulfocalix[4]-arene-nedaplatin complex. *J. Phys.: Conf. Ser.* **2019**, *1310*, 012011.

(11) Azzazy, H. M. E.-S.; Fahmy, S. A.; Mahdy, N. K.; Meselhy, M. R.; Bakowsky, U. Chitosan-Coated PLGA Nanoparticles Loaded with *Peganum harmala* Alkaloids with Promising Antibacterial and Wound Healing Activities. *Nanomaterials* **2021**, *11*, 2438.

(12) Fahmy, S. A.; Ramzy, A.; Mandour, A. A.; Nasr, S.; Abdelnaser, A.; Bakowsky, U.; Azzazy, H. M. E.-S. PEGylated Chitosan Nano-

particles Encapsulating Ascorbic Acid and Oxaliplatin Exhibit Dramatic Apoptotic Effects against Breast Cancer Cells. *Pharmaceutics* **2022**, *14*, 407.
(13) Fahmy, S. A.; Azzazy, H. M. E.-S.; Schaefer, J. Liposome Photosensitizer Formulations for Effective Cancer Photodynamic Therapy. *Pharmaceutics* **2021**, *13*, 1345.
(14) Fahmy, S. A.; Mahdy, N. K.; Al Mulla, H.; ElMeshad, A. N.; Issa, M. Y.; Azzazy, H. M. E.-S. PLGA/PEG Nanoparticles Loaded with Cyclodextrin-*Peganum harmala* Alkaloid Complex and Ascorbic Acid with Promising Antimicrobial Activities. *Pharmaceutics* **2022**, *14*, 142.
(15) Gou, M.; Wei, X.; Men, K.; Wang, B.; Luo, F.; Zhao, X.; Wei, Y.; Qian, Z. PCL/PEG copolymeric nanoparticles: potential nanoplatforms for anticancer agent delivery. *Curr. Drug Targets* **2011**, *12*, 1131−1150.
(16) Behl, A.; Parmar, V. S.; Malhotra, S.; Chhillar, A. K. Biodegradable diblock copolymeric PEG-PCL nanoparticles: Synthesis, characterization and applications as anticancer drug delivery agents. *Polymer* **2020**, *207*, 122901.
(17) Fahmy, S. A.; Mamdouh, W. Garlic oil−loaded PLGA nanoparticles with controllable size and shape and enhanced antibacterial activities. *J. Appl. Polym. Sci.* **2018**, *135*, 46133.
(18) Milosevic, M.; Stojanovic, D. B.; Simic, V.; Grkovic, M.; Bjelovic, M.; Uskokovic, P. S.; Kojic, M. Preparation and modeling of three-layered PCL/PLGA/PCL fibrous scaffolds for prolonged drug release. *Sci. Rep.* **2020**, *10*, 11126.
(19) Badran, M. M.; Alomrani, A. H.; Harisa, G. I.; Ashour, A. E.; Kumar, A.; Yassin, A. E. Novel docetaxel chitosan-coated PLGA/PCL nanoparticles with magnified cytotoxicity and bioavailability. *Biomed. Pharmacother.* **2018**, *106*, 1461−1468.
(20) Fahmy, S. A.; Issa, M. Y.; Saleh, B. M.; Meselhy, M. R.; Azzazy, H. M. E.-S. *Peganum Harmala* Alkaloids Self-Assembled Supramolecular Nanocapsules with Enhanced Antioxidant and Cytotoxic Activities. *ACS Omega* **2021**, *6*, 11954−11963.
(21) González-Forte, L. d. S.; Amalvy, J. I.; Bertola, N. Effect of natamycin on the physicochemical properties of corn starch based films and their effect on Penicillium spp. activity. *Int. J. Polym. Anal. Charact.* **2019**, *24*, 63−74.
(22) Aboeita, N. M.; Fahmy, S. A.; El-Sayed, M. M. H.; Azzazy, H. M. E.-S.; Shoeib, T. Enhanced Anticancer Activity of Nedaplatin Loaded onto Copper Nanoparticles Synthesized Using Red Algae. *Pharmaceutics* **2022**, *14*, 418.
(23) Fahmy, S. A.; Ramzy, A.; Sawy, A. M.; Nabil, M.; Gad, M. Z.; El-Shazly, M.; Aboul-Soud, M. A. M.; Azzazy, H. M. E.-S. Ozonated Olive Oil: Enhanced Cutaneous Delivery via Niosomal Nanovesicles for Melanoma Treatment. *Antioxidants* **2022**, *11*, 1318.
(24) Parsonidis, P.; Vlachou, I.; Mamagkaki, A.; Bouris, I.; Daikopoulou, V.; Papasotiriou, I. Cytotoxic effect of Boswellia sacra on human cancer cell lines. *J. Cancer Sci. Ther.* **2021**, *13*, 487.
(25) Zhao, X.; Wu, J.; Guo, D.; Hu, S.; Chen, X.; Hong, L.; Wang, J.; Ma, J.; Jiang, Y.; Niu, T.; Miao, F. Dynamic ginsenoside-sheltered nanocatalysts for safe ferroptosis-apoptosis combined therapy. *Acta Biomater.* **2022**, *151*, 549−560.
(26) Boonsongrit, Y.; Mueller, B. W.; Mitrevej, A. Characterization of drug−chitosan interaction by ^{1}H NMR, FTIR and isothermal titration calorimetry. *Eur. J. Pharm. Biopharm.* **2008**, *69*, 388−395.
(27) Khanal, S.; Adhikari, U.; Rijal, N. P.; Bhattarai, S. R.; Sankar, J.; Bhattarai, N. pH-Responsive PLGA Nanoparticle for Controlled Payload Delivery of Diclofenac Sodium. *J. Funct. Biomater.* **2016**, *7*, 21.
(28) Javaid, S.; Ahmad, N. M.; Mahmood, A.; Nasir, H.; Iqbal, M.; Ahmad, N.; Irshad, S. Cefotaxime Loaded Polycaprolactone Based Polymeric Nanoparticles with Antifouling Properties for In-Vitro Drug Release Applications. *Polymers* **2021**, *13*, 2180.
(29) Suhail, M. M.; Wu, W.; Cao, A.; Mondalek, F. G.; Fung, K. M.; Shih, P. T.; Fang, Y. T.; Woolley, C.; Young, G.; Lin, H. K. Boswellia sacra essential oil induces tumor cell-specific apoptosis and suppresses tumor aggressiveness in cultured human breast cancer cells. *BMC Complementary Altern. Med.* **2011**, *11*, 129.
(30) Frank, M. B.; Yang, Q.; Osban, J.; Azzarello, J. T.; Saban, M. R.; Saban, R.; Ashley, R. A.; Welter, J. C.; Fung, K. M.; Lin, H. K. Frankincense oil derived from Boswellia carteri induces tumor cell specific cytotoxicity. *BMC Complementary Altern. Med.* **2009**, *9*, 6.
(31) Yazdanpanahi, N.; Behbahani, M.; Yektaeian, A. Effect of boswellia thurifera gum methanol extract on cytotoxicity and p53 gene expression in human breast cancer cell line. *Iran. J. Pharm. Res.* **2014**, *13*, 719−724.
(32) Sanna, V.; Roggio, A. M.; Posadino, A. M.; Cossu, A.; Marceddu, S.; Mariani, A.; Alzari, V.; Uzzau, S.; Pintus, G.; Sechi, M. Novel docetaxel-loaded nanoparticles based on poly(lactide-co-caprolactone) and poly(lactide-co-glycolide-co-caprolactone) for prostate cancer treatment: formulation, characterization, and cytotoxicity studies. *Nanoscale Res. Lett.* **2011**, *6*, 260.
(33) Jo, H.; Cha, B.; Kim, H.; Brito, S.; Kwak, B. M.; Kim, S. T.; Bin, B.-H.; Lee, M.-G. α-Pinene Enhances the Anticancer Activity of Natural Killer Cells via ERK/AKT Pathway. *Int. J. Mol. Sci.* **2021**, *22*, 656.
(34) Araújo-Filho, H. G.; dos Santos, J. F.; Carvalho, M. T. B.; Picot, L.; Fruitier-Arnaudin, I.; Groult, H.; Quintans-Júnior, L. J.; Quintans, J. S. S. Anticancer activity of limonene: A systematic review of target signaling pathways. *Phytother. Res.* **2021**, *35*, 4957−4970.
(35) Zhang, W.; Zhao, X.; Yuan, Y.; Miao, F.; Li, W.; Ji, S.; Huang, X.; Chen, X.; Jiang, T.; Weitz, D. A.; Song, Y. Microfluidic Synthesis of Multimode Au@CoFeB-Rg3 Nanomedicines and Their Cytotoxicity and Anti-Tumor Effects. *Chem. Mater.* **2020**, *32*, 5044−5056.

https://doi.org/10.1021/acsomega.2c06390
ACS Omega 2023, 8, 1017−1025